Hyperfine Interactions **153:** 43–55, 2004.

^{166}Er and ^{170}Yb Mössbauer Studies of Magnetic Order and Valence

D. H. RYAN[1] and J. M. CADOGAN[2]
[1] *Physics Department and Centre for the Physics of Materials, McGill University, 3600 University Street, Montreal, PQ H3A 2T8, Canada*
[2] *School of Physics, The University of New South Wales, Sydney, NSW 2052, Australia*

Abstract. We present three case studies of magnetic ordering in Er and Yb intermetallic compounds ($ErFe_6Sn_6$, Er_3Ge_4 and $YbMn_2Si_{2-x}Ge_x$). Mössbauer measurements of electric field gradients and hyperfine fields at the rare-earth sites provide direct, local information which yields insight beyond that which could be obtained using neutron diffraction. We argue that such Mössbauer work is an ideal complement to bulk studies.

Key words: ytterbium, erbium, rare-earths, intermetallic compounds, magnetic order, valence.

1. Introduction

While neutron diffraction remains the method of choice for investigating magnetic order in rare-earth intermetallics, its blanket sensitivity to all structural and magnetic changes occurring in the sample can make interpretation of the data quite challenging. This is especially true when two or more magnetic species are present, or when structure factor effects lead to weak or highly distributed magnetic scattering. In addition, small amounts of impurities may lie undetected among the stronger scattering of the primary phase, but may still contribute a temperature dependent scattering if they order. Finally, as there is no charge sensitivity in the neutron scattering cross section, it is effectively blind to valence state or changes in valence.

By contrast, Mössbauer spectroscopy provides a local probe of magnetic order that is exquisitely sensitive to structure, magnetic order and valence. The information comes from a specific element (strictly speaking, a specific isotope of that element) in the compound, and provides direct information on the behaviour and environment of that element, and indirect information on the behaviour of its first neighbours. In the case studies that follow, we will show how data from Mössbauer spectroscopy has been used to develop a much clearer understanding of the magnetic ordering in three distinct materials. In doing this, we in no way intend to argue that Mössbauer spectroscopy should replace neutron diffraction; indeed all of the systems presented here have been actively studied by neutron diffraction. We wish rather to demonstrate that neutron diffraction should not be used in isolation,

and that by bringing more than one technique to bear on a problem, a much clearer and unambiguous picture emerges.

2. Experimental methods

The samples were prepared by arc melting under Ti-gettered argon using stoichiometric amounts of Mn (99.99%), Fe (99.99%), Si (99.999%), Ge (99.999%), Sn (99.99%), Er (99.9%) and Yb (99.9%). The samples were annealed under vacuum, and then examined using Cu K_α X-ray diffraction. Magnetisation measurements were carried out on a Quantum Design PPMS susceptometer/magnetometer in fields of up to 9 Tesla.

Neutron powder diffraction experiments were carried out on $\sim 6g$ samples of $ErFe_6Sn_6$ on the E9 Fine Resolution Powder Diffractometer (FIREPOD [1]) at the BENSC reactor, Hahn-Meitner Institute, Berlin, Germany, using a neutron wavelength of 1.5831(1) Å. All diffraction patterns (both X-ray and neutron) were analysed using the Rietveld method and the GSAS program [2].

^{57}Fe and ^{119}Sn Mössbauer spectroscopy was carried out in conventional, constant-acceleration, transmission mode with standard ^{57}Co**Rh** and ^{119m}Sn:$BaSnO_3$ sources, respectively. In both cases, the spectrometer was calibrated against a 99.99% α-Fe foil using the ^{57}Co**Rh** source.

The sources for ^{166}Er Mössbauer spectroscopy were made by neutron irradiation of $Ho_{0.4}Y_{0.6}H_2$ at the SLOWPOKE Reactor Laboratory, Ecole Polytechnique Montréal, Québec, to produce $\sim$1 GBq initial activity of the 27-hour ^{166}Ho parent isotope. The spectrometer was operated vertically with both source and sample cooled in a helium-flow cryostat and gave a linewidth of 2.49(4) mm/s (HWHM) for an $ErFe_2$ standard at 4.5 K. Independent temperature control of the source was used to keep it at or above 5 K to avoid relaxation-induced line broadening which we have observed at lower source temperatures. A He/Ne laser interferometer was used to provide simultaneous calibration of all spectra. Velocity calibration was cross-checked using the 819.4 T magnetic splitting in $ErFe_2$ (this being the average ^{166}Er Mössbauer measurement of 820.5(8) T by Hodges *et al.* [3] and the ^{167}Er NMR measurement of 818.4 $\pm$ 10 T by Berthier and Devine [4]). The spectra were fitted using a conventional nonlinear least-squares minimisation routine with line positions and intensities derived from a full solution to the nuclear hyperfine Hamiltonian for the ^{166}Er $2 \rightarrow 0$ transition.

The 0.4 GBq ^{170}Tm source used for ^{170}Yb Mössbauer spectroscopy was prepared by neutron activation of $\sim$25 mg of Tm as a 10 wt% alloy in aluminium at the McMaster Nuclear Reactor, Hamilton, Ontario. The experimental arrangement was the same as that used for the ^{166}Er work, except that the laser calibration was cross-checked against a 99.99% α-Fe foil. Spectrum fitting procedure was the same as that used for ^{166}Er. The 80.6 keV ^{166}Er and 84.3 keV ^{170}Yb γ-rays were detected using a high-purity Germanium detector.

3. $ErFe_6Sn_6$

The magnetic moments on the rare-earth (R) and Fe sublattices in the RFe_6Sn_6 intermetallic compounds order independently of one another in those compounds where the R^{3+} ion has a magnetic moment [5]. The Fe sublattice orders antiferromagnetically with a Néel temperature (T_N) which remains essentially constant at ∼555 K across the whole series. Neutron powder diffraction shows that the easy direction of magnetic order of the Fe sublattice is [1 0 0] in the orthorhombic setting. For R = Gd–Er, the rare-earth sublattice orders at much lower temperatures, ranging from 45 K for $GdFe_6Sn_6$ to 4.8 K for $ErFe_6Sn_6$, without affecting the Fe order. The magnetic independence of the R and Fe sublattices is related to the layered structure of these compounds which are formed by placing rare-earth atoms between the hexagonal Fe planes of the parent FeSn (B35) structure. Binary FeSn consists of ferromagnetic Fe planes coupled antiferromagnetically to each other [6, p. 47; 7] and there is a net cancellation of the Fe–R magnetic exchange at the interplanar R sites, effectively isolating the rare-earth from the ordering of the iron moments.

Room temperature ^{57}Fe and ^{119}Sn Mössbauer spectroscopy (Figure 1) confirms the magnetic structure of the Fe sublattice derived from neutron diffraction. The average ^{57}Fe hyperfine field B_{hf} is 20.1(1) T at 295 K and 22.9(3) T at 12 K.

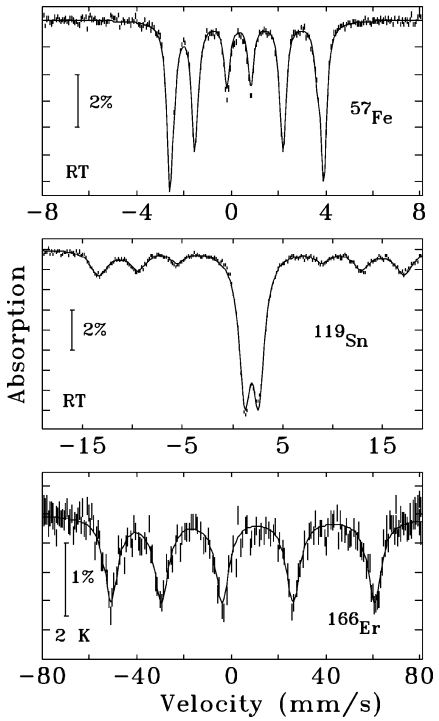

Figure 1. ^{57}Fe (top), ^{119}Sn (middle) and ^{166}Er (bottom) Mössbauer spectra of $ErFe_6Sn_6$ obtained at 295 K (^{57}Fe and ^{119}Sn) and 2 K (^{166}Er). Note the different velocity scales of these three spectra.

This latter value translates into an Fe moment of 2.0(5) μ_B at 12 K, using the field-to-moment conversion factor of 11.2 ± 2.5 T/μ_B [6, p. 55], fully consistent with the 2.4(6) μ_B derived from our neutron diffraction data at 5.3 K. Note that essentially all of the uncertainty on the moment derived from the Mössbauer data is associated with the field-to-moment conversion factor.

Sn is non-magnetic and so any hyperfine magnetic field observed at the ^{119}Sn nucleus is due to surrounding magnetic moments, i.e., a transferred hyperfine field. Above ~5 K only the Fe sublattice is magnetically ordered and its magnetic structure, determined from our neutron diffraction data, indicates that the eight Sn 4c sites have half of their neighbouring Fe moments along [1 0 0] and half antiparallel along [$\bar{1}$ 0 0], resulting in a zero transferred hyperfine field. However, the two Sn 8g sites, which account for exactly $\frac{1}{3}$ of the Sn atoms, have all their neighbouring Fe moments parallel, which should result in a substantial transferred hyperfine field. Figure 1 shows that the ^{119}Sn Mössbauer spectrum of $ErFe_6Sn_6$ at 295 K comprises both a magnetically-split and a non-magnetic component, and the fit shows that 36(2)% of the Sn sites have a transferred hyperfine field of 22.2(1) T, whereas the remaining 64(2)% of the Sn sites experience no net transferred hyperfine field, in excellent agreement with our deduced magnetic structure of the Fe sublattice in $ErFe_6Sn_6$.

While the Fe magnetic structure is clear, and the Mössbauer data simply provide confirmation of the analysis, the situation for the Er ordering is more complex. Figure 2 shows the neutron diffraction patterns obtained above and below the 4.8 K ordering of the Er moments. It is immediately apparent that very little changes. Indeed, the strongest purely magnetic peak at $2\theta = 11.95°$ has an intensity of less than 100 counts: comparable to the $\sqrt{N}$ uncertainty on the strongest nuclear peak which has an intensity of ~13,000 counts. This magnetic peak corresponds to (hkl) = (1 $\frac{5}{2}$ 0), indicating a doubling of the magnetic cell along the crystal *b*-axis, associated with the antiferromagnetic component of the Er order. There are also magnetic contributions to nuclear peaks, and the combination of our neutron scattering and magnetization data shows that the Er magnetic order comprises both ferromagnetic (FM) and antiferromagnetic (AF) components, a situation similar to that recently found in $HoFe_6Sn_6$ [8]. Analysis of the magnetic scattering from the Er moments shows the ferromagnetic ordering of the Er to be along [1 0 0] while the antiferromagnetic ordering is along [0 1 0]. The fitted moment components are: $Er^{FM} = 2.6 \pm 1.0\ \mu_B$ and $Er^{AF} = 4.9 \pm 1.5\ \mu_B$, giving a net Er moment of only $5.5 \pm 1.8\ \mu_B$. There are two significant problems with these results. Firstly, the total Er moment is little more than half of the 9 μ_B that would be expected, and secondly, the deduced FM component is not consistent with the value of 5.9(1) μ_B obtained from magnetisation measurements.

The problem almost certainly lies with the Er^{FM} component, as its contribution to the observed scattering will appear only at existing allowed nuclear Bragg peaks, and the induced intensity changes are unlikely to significantly exceed the statistical uncertainties on those peaks. We therefore turn to ^{166}Er Mössbauer spectroscopy to

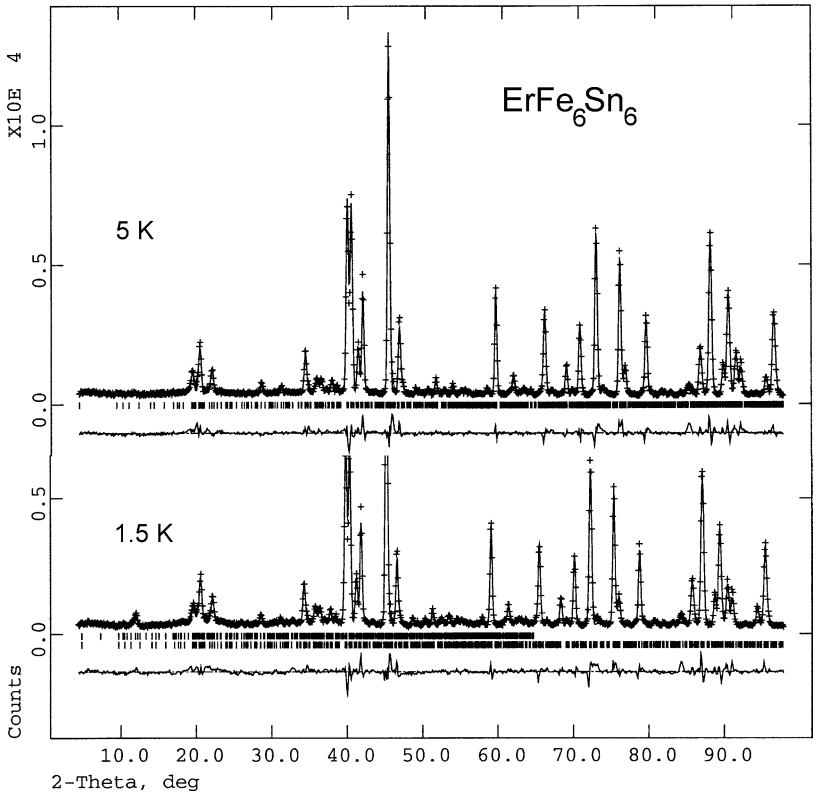

Figure 2. Neutron powder diffraction patterns of $ErFe_6Sn_6$ obtained with $\lambda = 1.5831(1)$ Å. Top: at 5 K (above the Er ordering temperature); bottom: at 1.5 K (below the ordering temperature of the Er moments). The peak at $2\theta = 11.95°$ in the 1.5 K pattern is the strongest, purely magnetic feature.

check the total Er moment. The bottom panel of Figure 1 shows the ^{166}Er data taken at 2 K – a well-resolved magnetically-split pentet, despite the fact that there are two inequivalent Er sites in the $ErFe_6Sn_6$ structure. This immediately supports our use of a single Er magnetic moment in the fitting of the neutron diffraction data. The experimental half-linewidth is 3.5(1) mm/s, broader than the source linewidth of 2.49(4) mm/s on the $ErFe_2$ calibration. This broadening most likely reflects the fact that the $ErFe_6Sn_6$ structure actually contains two crystallographically inequivalent Er sites which are unresolved by ^{166}Er Mössbauer spectroscopy, but it may also include the effects of residual slow electronic relaxation. The hyperfine magnetic field (B_{hf}) at the ^{166}Er nucleus in $ErFe_6Sn_6$ at 2 K is 742(5) T.

B_{hf} at a rare-earth site in an R–Fe intermetallic compound can be written as [9]

$$B_{hf} = B_{4f} + B_{cp} + B_p + B_{nn}^{R} + B_{nn}^{Fe} + B_{ext}, \tag{1}$$

where both B_{4f} and B_{cp} can be expressed in terms of $\langle J_Z \rangle$. Li *et al.* [10] deduced a value of 770.0 ± 7.4 T for the total intra-ionic hyperfine field (i.e., $B_{4f} + B_{cp}$) in $ErFe_2$, implying a moment to field conversion factor of 85.6(8) T/μ_B.

B_p is the contribution from conduction electron polarization by the spin of the parent R^{3+} ion, and is given by

$$B_p = K_p\langle S_Z\rangle = K_p(g_J - 1)\langle J_Z\rangle, \tag{2}$$

where K_p is a constant. The contribution of this term can also be estimated from the work of Li *et al.* [10] who deduce a value of 9.4 ± 1.4 T for K_p in $ErFe_2$. $g_J = 1.2$ and $\langle J_Z\rangle = 9$ gives $B_p = 14.1 \pm 2.1$, for a total field in a metallic environment of 784.1 ± 7.7 T and a moment to field conversion factor of 87.1 ± 1.2 T/μ_B.

B_{nn}^R and B_{nn}^{Fe} are transferred hyperfine fields from the surrounding R and Fe sublattices, respectively. B_{nn}^R can estimated by noting that our magnetization measurement yields a ferromagnetic Er moment component of 5.9 μ_B per Er^{3+} ion. The corresponding field in $ErFe_2$ is 5.1 ± 1.3 T [10] for an Er^{3+} moment of 9 μ_B and if we assume that this transferred field scales with the Er sublattice magnetization, we obtain a value of 0.7 T for B_{nn}^{Er} in $ErFe_6Sn_6$. The transferred hyperfine field from the Fe sublattice (B_{nn}^{Fe}) is zero since the Fe sublattice is antiferromagnetic and the Er and Fe sublattices are magnetically independent.

Finally, we have no externally applied magnetic fields, so B_{ext} is zero.

Thus, our experimentally determined ^{166}Er hyperfine magnetic field value of 742(5) T, corrected for B_p and B_{nn}^{Er}, translates to $\langle J_Z\rangle = 7.1$ which corresponds to a total Er^{3+} magnetic moment of 8.5(1) μ_B. This value is significantly larger than the 5.5 ± 1.8 μ_B determined by neutron diffraction alone. However, as discussed earlier, the *ferromagnetic* component of the Er^{3+} moment is more reliably determined from our magnetization measurements (5.9 ± 0.1 μ_B). Combining *this* value with the antiferromagnetic component provided directly by neutron diffraction (4.9 ± 1.5 μ_B) yields a total Er^{3+} moment of 7.7 ± 1.7 μ_B, which is fully consistent with our direct determination of 8.5(1) μ_B by ^{166}Er Mössbauer spectroscopy. Alternatively, if we combine our most accurate determinations (total from B_{hf} and ferromagnetic from magnetization) we obtain 6.12 ± 0.12 μ_B for the antiferromagnetic component.

It is clear from this exercise, that while neutron diffraction is probably the only way to determine the magnetic structure of a material, especially when the structure is as complex as that of $ErFe_6Sn_6$, it is not always the most accurate way to obtain actual moments.

4. Er_3Ge_4

Analysis of neutron diffraction data below the Néel temperature (T_N) of 7.3 K revealed a two-dimensional canted antiferromagnetic triangular structure with very different moments associated with the two crystallographically distinct Er sites [11]. At 1.5 K these were reported to be 7.32(5) μ_B/Er at the Er_1(8f) site, and 6.37(6) μ_B/Er at the Er_2(4c) site [11]. In addition, distinct temperature dependences were found for the two Er sites, with the Er–4c moment falling much more rapidly than the Er–8f moment. Finally, a weak ($\sim 1^\circ$) spin reorientation was claimed to

occur at the 8f site around 4 K associated with a slight change in the temperature dependence of the Er_2(4c) moment. Two calorimetric studies of Er_3Ge_4 have been made [12, 13]. Janssen *et al.* [12] reported a sharp peak at 6.9 K, corresponding to T_N and a weak shoulder around 4 K which they associated with the spin reorientation seen by neutron scattering. They commented that their integrated magnetic entropy is rather low, but their plotted heat capacity data for Er_3Ge_4 lie far below that reported by the same group for the non-magnetic analogue Lu_3Ge_4 [14]. By contrast, a more recent calorimetric study [13] revealed two clear features in the low-temperature heat capacity. The upper one ($\sim$7 K) is clearly associated with the onset of antiferromagnetic order, and the second peak at $\sim$3.5 K was linked to the spin reorientation at 4 K reported in the neutron diffraction study [11]. While the total entropy change below T_N in this latter study appears quite reasonable, the entropy associated with the 3.5 K peak is remarkably large, accounting for about a third of the total entropy change observed between 0 K and T_N (7.3 K). The size of the peak at $\sim$3.5 K suggests either the presence of a magnetic impurity (which would bring it more into line with the earlier work [12]), or that far more than just a 1° spin reorientation occurs at 3.5 K in Er_3Ge_4.

The ^{166}Er Mössbauer spectrum of Er_3Ge_4 at 2.5 K (Figure 3) shows that the two Er sites are fully resolved, exhibiting quite different magnetic hyperfine fields, as expected from the earlier neutron diffraction data [11]. Four of the five magnetic lines clearly have two components (the central line results from the $0 \rightarrow 0$ hyperfine transition and is not affected by a magnetic hyperfine field), and the fitted area of the more widely split pentet between 1.5 K and 6 K is $65.2 \pm 2.3\%$ of the total area, fully consistent with the 2 : 1 ratio expected for Er in the 8f:4c sites. This clear agreement on the relative areas of the two subspectra permits unambiguous assignment of each component to Er atoms in specific crystallographic sites. The two hyperfine fields at 1.5 K are 654(1) T for the 8f site and 553(2) T for the 4c site,

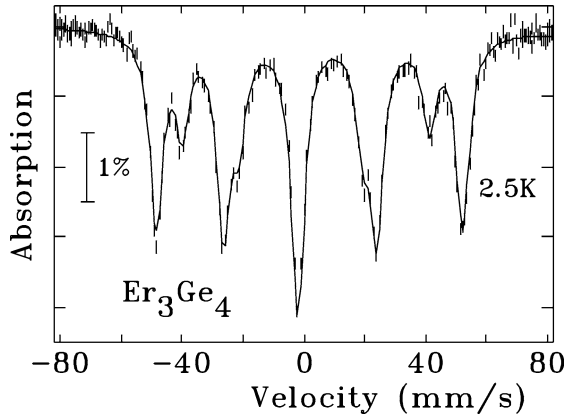

Figure 3. ^{166}Er Mössbauer spectrum of Er_3Ge_4 taken at 2.5 K, well below T_N. The magnetic pentets from the two Er sites are clearly resolved.

giving a field ratio of 1.183(5) : 1, which compares extremely well with the moment ratio of 1.15(2) : 1 determined by neutron diffraction at the same temperature [11]. These fields (and the neutron derived Er moments) are far smaller than those expected for Er in an antiferromagnetic, metallic environment (see Equation (1) and discussion following it in the previous section) in a pure 15/2 ground state; therefore there must be a substantial crystal-field induced admixture of other states, even at 1.5 K. Reduced Er moments appear to be a common feature of binary Er–Ge alloys [15].

Visual inspection of the two components in the Mössbauer spectra reveals that they have very different temperature dependences, with the 8f subspectrum remaining essentially unchanged, while the 4c subspectrum collapses rapidly with increasing temperature. This behaviour is summarised in Figure 4 where the B_{hf} at the two sites are plotted versus temperature.

The ratio between our average hyperfine field and the reported Er moment [11] at 1.5 K is 88.3 ± 0.5 T/μ_{B} (where the error comes almost entirely from uncertainties in the neutron diffraction moments), in complete agreement with our conversion factor of 87.1 ± 1.2 T/μ_{B} derived above for an antiferromagnetic metallic environment. This scaling factor allows us to make a direct comparison between our measured hyperfine fields at the two Er sites, and the two neutron diffraction derived moments [11] (open symbols in Figure 4). The absolute agreement at 1.5 K is excellent; however, B_{hf} at the 8f site shows very little temperature dependence. By contrast, B_{hf} at the 4c site tracks the reported temperature dependence of the Er moment at that site remarkably well, with one important difference: we see no evidence of the decrease at 4 K deduced from analysis of the neutron diffraction data [11], and attributed to the spin reorientation. Given the excellent overall

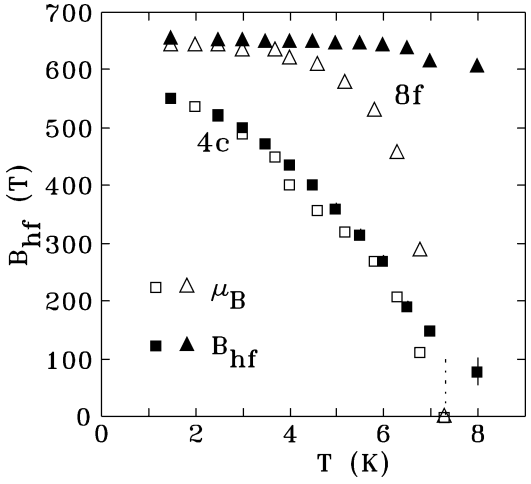

Figure 4. Temperature dependence of the ^{166}Er hyperfine fields at the two Er sites in Er_3Ge_4 (solid symbols). For comparison, the Er moments derived from neutron diffraction data [11] are shown as open symbols, scaled by a factor of 87.1 T/μ_{B} (see text). The dotted line at 7.3 K marks T_{N}.

agreement, and the enhanced precision provided by the ^{166}Er Mössbauer measurements compared with neutron diffraction, the absence of a break in slope in $B_{hf}(T)$ for the 4c site is highly significant. Within the uncertainty of our measurements (<0.4%), there is no change in B_{hf} at the 4c site, beyond the expected smooth thermal evolution. Our ^{166}Er Mössbauer spectra provide clear confirmation of the reduced Er moments and their distinct temperature dependences, but the spectra show no changes around 4 K that we could associate with a spin reorientation, or any other change in the intrinsic magnetic order.

The excellent agreement on the behaviour of the moment at the 4c site both above and below the 4 K event, coupled with the break in slope in the neutron diffraction data being close to the reported uncertainties would suggest that interpretation of the diffraction data in terms of a spin reorientation may be equivocal. Such a view would be more consistent with a heat capacity measurement that shows only a weak shoulder around 4 K [12], and not with data exhibiting a large peak [13]. The complexity of the Er–Ge binary phase diagram coupled with the fact that none of the binary phases around Er_3Ge_4 melts congruently [16] makes some level of impurity almost inevitable. Indeed, none of our Er–Ge alloys were completely single-phase, and the sample of Er_3Ge_4 used in this study contained a ~5 wt.% ErGe impurity. Since we were unable to locate complete data on magnetic transition temperatures in the Er–Ge binary alloy system that would allow us to associate a specific contaminant with the event at ~4 K, we prepared samples of the two neighbouring phases: ErGe, slightly richer in Er and known to occur as a contaminant in our own sample, and Er_2Ge_3 slightly poorer in Er. While we found that ErGe orders at 6.6(2) K, and therefore could not be the impurity we seek, Figure 5 shows that Er_2Ge_3 orders at 4.0 ± 0.1 K and lines up nicely with

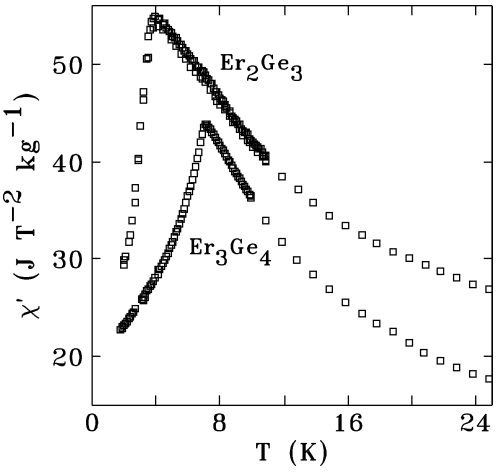

Figure 5. Temperature dependence of the ac-susceptibility (χ') for Er_3Ge_4 and Er_2Ge_3 showing cusps at $T_N = 7.3 \pm 0.1$ K and 4.0 ± 0.1 K, respectively. The break in the Er_2Ge_3 data at 7 K reflects the presence of a ~10 wt.% Er_3Ge_4 in this sample.

the peak reported in the specific heat capacity [13]. Er_2Ge_3 is extremely close in composition to Er_3Ge_4 (40 at.% Er vs. 43 at.%), and is certainly present in the as-cast ingot. Furthermore, some erbium loss is inevitable on both melting and subsequent annealing. If the initial erbium excess used in the ingot were too small, such a loss of erbium would lead to retention of Er_2Ge_3 from the original casting, or even formation of new Er_2Ge_3. Differing levels of Er_2Ge_3 impurities could easily account for the differences between the two calorimetric studies [12, 13], and the additional magnetic scattering that develops as Er_2Ge_3 orders might account for the apparent spin reorientation seen in the neutron diffraction data [11]. However a re-analysis of those data would be needed to properly address this possibility.

5. $YbMn_2Si_{2-x}Ge_x$

$YbMn_2Ge_2$ and $YbMn_2Si_2$ have been shown to exhibit complex magnetic ordering associated with both the Mn and Yb sublattices [17]. More recent neutron diffraction work has elucidated the detailed behaviour in each case. $YbMn_2Ge_2$ is a planar antiferromagnet below $T_N = 510$ K and undergoes a spin canting starting at ~185 K [18]. Ytterbium is expected to be essentially divalent in this compound and hence non-magnetic. Thus all magnetic order in $YbMn_2Ge_2$ derives from the Mn moments. Analysis of the cell volume has led to the suggestion that the Yb atoms may depart from a pure Yb^{2+} charge state and have a valence of 2.35 [19]. $YbMn_2Si_2$ follows a similar pattern except that when the Mn moments order below $T_N = 526$ K, they adopt an axial antiferromagnetic state [20]. Previous work attributed a second transition at ~35 K to ordering of trivalent Yb [17], however this was not confirmed by neutron diffraction which showed that this event corresponds to a rearrangement of the Mn moments into a cell-doubled antiferromagnetic state [20]. Ordering of the Yb moments was not seen to occur until close to 1.5 K.

The primary issue to be dealt with here is the valence of the Yb in the two compounds. Both crystallise in the body centred tetragonal $ThCr_2Si_2$-type structure (I4/mmm), which has a single Yb site. While the magnetic structure of $YbMn_2Ge_2$ changes from layered planar to a canted structure below ~185 K [18], the environment of the Yb atoms is such that no net transferred field is expected at any temperature. By contrast, the change in the Mn moment arrangement in $YbMn_2Si_2$ at ~35 K [20] leads to a cell-doubling and two magnetically inequivalent Yb sites, only one of which should experience a transferred field from neighbouring Mn moments. We therefore examined the valence by comparing spectra in magnetically simple states.

The ^{170}Yb Mössbauer spectrum of $YbMn_2Ge_2$ at 4.5 K shown in Figure 6 is characteristic of divalent Yb. It exhibits a slightly asymmetric line reflecting a small ($+3.5 \pm 0.1$ mm/s) unresolved quadrupole splitting, essentially zero isomer shift (-0.04 ± 0.02 mm/s) and no hyperfine magnetic field. While the isomer shifts are always small for ^{170}Yb, the value found here in $YbMn_2Ge_2$ is typical of divalent Yb in a metallic environment [21]. Furthermore, the small quadrupole

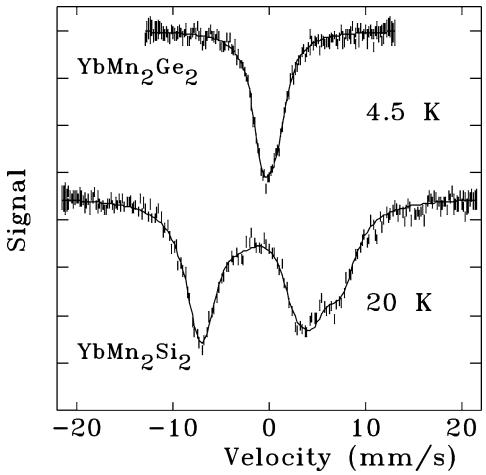

Figure 6. ^{170}Yb Mössbauer spectra of $YbMn_2Ge_2$ at 4.5 K (top) and $YbMn_2Si_2$ at 20 K (bottom).

splitting is similar to that seen in other divalent Yb alloys such as the Yb–Cd system [22] and suggests that the 4f shell is full. There is no indication of the additional quadrupole splitting that would be associated with even a partial hole in the 4f shell (removing one electron from the 4f shell without changing the crystal structure leads to a ∼30 mm/s change in the quadrupole splitting – see $YbMn_2Si_2$ below). We therefore find no evidence to support the valence of 2.35 inferred from the cell volume in recent neutron diffraction work [19]. By contrast, $YbMn_2Si_2$ at 20 K has a substantial and well-resolved quadrupole splitting of -28.6 ± 0.2 mm/s. While 20 K is below the Mn cell-doubling event and so a small transferred hyperfine field of 15(3) T is present, the recoil free fraction is much higher here at 20 K, than at 40 K (above the cell-doubling event where the field is zero) and the cleaner signal simplifies the analysis. Yb is clearly trivalent in this alloy.

Analysis of lattice parameters in neutron diffraction patterns at the Ge-rich end of the $YbMn_2Si_{2-x}Ge_x$ series suggests that there is a coexistence region where both divalent and trivalent ytterbium forms of the compound are present. Neutron data taken at 250 K indicate that the Yb^{2+} form starts to appear for $x \geqslant 1.6$ with the two valence forms being present at $x = 1.8$ [23]. However, preliminary analysis of our 4.5 K ^{170}Yb Mössbauer data shows that divalent ytterbium is present as early as $x = 1.2$. One possible explanation for this discrepancy could be that the Yb^{2+} fraction is temperature dependent. Figure 7 shows that this is indeed the case, and that the Yb^{2+} component is lost on heating. A linear fit to the data in Figure 7 suggests that $YbMn_2Si_{0.6}Ge_{1.4}$ would contain only trivalent ytterbium above ∼180K, fully consistent with the boundary of $x \sim 1.6$ inferred from neutron diffraction at 250 K.

Finally, we turn briefly to the question of ordering of the Yb^{3+} moments in $YbMn_2Si_2$. This compound already has a checkered history, with the 35 K event originally being attributed to ordering of Yb^{3+} moments [17] but subsequently

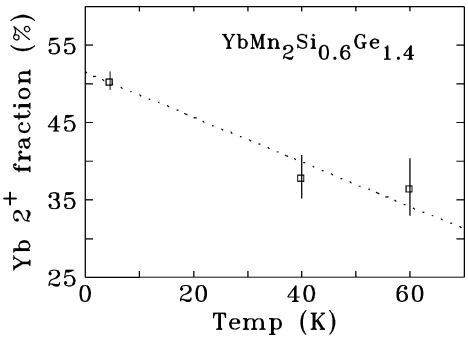

Figure 7. Fraction of ytterbium present as Yb^{2+} as a function of temperature for $YbMn_2Si_{0.6}Ge_{1.4}$ showing a gradual decrease on heating. Dotted line is a linear fit intended as a guide to the eye.

being shown to reflect a change in the ordering of the Mn moments [20]. The temperature dependence of the transferred hyperfine field in $YbMn_2Si_2$ shows only a weak linear increase below 40 K. B_{hf} is small, and the fitted onset is 38(2) K, consistent with the field being due to the rearrangement of the Mn moments detected by neutron diffraction [20]. However, there is no change in the temperature dependence on further cooling and even by 1.6 K the ^{170}Yb field is only 35(2) T, a value that is not consistent with ordering of the Yb sublattice. Our ^{170}Yb Mössbauer data do not therefore provide any support for ordering of Yb^{3+} moments above 1.6 K in $YbMn_2Si_2$.

6. Conclusions

^{166}Er and ^{170}Yb Mössbauer spectroscopy provides extremely useful information on the magnetic ordering of the rare-earths in intermetallic compounds. In the case studies presented here we have: (i) obtained an accurate value for the total Er moment in $ErFe_6Sn_6$ and so cross-checked neutron diffraction data, (ii) confirmed that very different Er moments are present on the two inequivalent sites in Er_3Ge_4, but found no evidence for a spin reorientation, (iii) mapped out the Yb^{2+}/Yb^{3+} boundary in $YbMn_2Si_{2-x}Ge_x$ and shown that there is no evidence for ordering of Yb^{3+} moments above 1.6 K.

Acknowledgements

This work was supported by grants from the Natural Sciences and Engineering Research Council of Canada, Fonds pour la formation de chercheurs et l'aide à la recherche, Québec, the Australian Nuclear Science and Technology Organisation, the Australian Academy of Science, the Australian Research Council.

Various parts of this work were carried out on reciprocal sabbatical visits, therefore, J.M.C. wishes to acknowledge the hospitality of the Centre for the Physics of Materials, Department of Physics, McGill University, Montreal, Canada, while

D.H.R. wishes to acknowledge the hospitality of the School of Physics, The University of New South Wales, Sydney, Australia. The authors are grateful to Greg Kennedy and the staff of the SLOWPOKE Reactor Laboratory at Ecole Polytechnique Montréal, Québec, and to Mike Butler and the staff of the McMaster Nuclear Reactor, Hamilton, Ontario, where the activation of the sources used in this work was carried out.

We are grateful to O. Moze, M. Hofmann, S. J. Campbell, A. V. J. Edge, R. Gagnon, N. M. Saleema and M. Elouneg-Jamróz for assistance with some of the measurements, and for many enlightening discussions.

References

1. Többens, D. M. and Stüßer, N., *Neutron News* **12**(3) (2001), 28.
2. Larson, A. C. and von Dreele, R. B., 1985–94, Los Alamos National Laboratory, Report LAUR 86-748 (1994) (unpublished).
3. Hodges, J. A., Jehanno, G., Schuhl, A. and Berthier, Y., *Hyp. Interact.* **11** (1981), 29.
4. Berthier, Y. and Devine, R. A. B., *J. Appl. Phys.* **52** (1981), 2071.
5. Cadogan, J. M. and Ryan, D. H., *J. Alloys Compounds* **326** (2001), 166.
6. Häggström, L., Ericsson, T., Wäppling, R. and Chandra, K.: *Phys. Scripta* **11** (1975), 47, 55.
7. Beckman, O., Carrander, K., Lundgren, L. and Richardson, M., *Phys. Scripta* **6** (1972), 151.
8. Cadogan, J. M., Suharyana, Ryan, D. H., Moze, O. and Kockelmann, W., *IEEE Trans. Mag.* **37** (2001), 2606.
9. Cadogan, J. M. and Ryan, D. H., *Hyp. Interact.* (this issue).
10. Li, Y., Carboni, C., Ross, J. W., McCausland, M. A. H. and Bunbury, D. St. P., *J. Phys. Condens. Matter* **8** (1996), 865.
11. Schobinger-Papamantellos, P., Oleksyn, O., Ritter, C., de Groot, C. H. and Buschow, K. H. J., *J. Magn. Magn. Mater.* **169** (1997), 253.
12. Janssen, Y., Brück, E., Kayzel, F. E., de Boer, F. R., Buschow, K. H. J., Oleksyn, O. and Schobinger-Papamantellos, P., *J. Magn. Magn. Mater.* **177–181** (1998), 1147.
13. Chen, Y. Y., Yao, Y. D., Lin, Y. S., Chang, C. L., Hamdeh, H. H. and Ho, J. C., *Phys. Rev. B* **61** (2000), 58.
14. Zaharko, O., Schobinger-Papamantellos, P., Sikora, W., Ritter, C., Janssen, Y., Brück, E., de Boer, F. R. and Buschow, K. H. J., *J. Phys. Condens. Matter* **10** (1998), 6553.
15. Ryan, D. H., Cadogan, J. M. and Gagnon, R. (unpublished results).
16. Massalski, T. B., Murray, J. L., Bennett, L. H. and Baker, H. (eds), *Binary Alloy Phase Diagrams*, Amer. Soc. Metals, Metals Park, Ohio, 1986.
17. Nowik, I., Felner, I. and Bauminger, E. R., *J. Magn. Magn. Mater.* **185** (1998), 91.
18. Hofmann, M., Campbell, S. J. and Szytula, A., *J. Alloys Compounds* **311** (2000), 137.
19. Hofmann, M., Campbell, S. J. and Edge, A. V. J., *Appl. Phys. A* (in press).
20. Hofmann, M., Campbell, S. J., Edge, A. V. J. and Studer, A. J., *J. Phys. Condens. Matter* **13** (2001), 9773.
21. Bauminger, E. R., Kalvius, G. M. and Nowik, I., In: Shenoy, G. K. and Wagner, F. E. (eds), *Mössbauer Isomer Shifts*, North-Holland, Amsterdam, 1978, p. 660.
22. Ryan, D. H., Saleema, N. M., Gagnon, R. and van Lierop, J., *J. Phys. Condens. Matter* **13** (2001), 10159.
23. Hofmann, M. *et al.* (unpublished results).